LINE SOURCE SCATTERING BY A RIDGE ON A METAL PLANE

Danilo Erricolo, Piergiorgio L.E. Uslenghi, Badria Elnour
Department of Electrical and Computer Engineering
University of Illinois at Chicago
851 South Morgan Street
Chicago, IL 60607-7053 USA
email: erricolo@ece.uic.edu, uslenghi@uic.edu, belnou2@uic.edu

ABSTRACT
The scattering from a metal plane with a ridge is considered in the case of line source illumination and for two polarizations. Exact analytical results are expressed using series that contain products of radial and angular Mathieu functions. The exact analytical results are computed and compared with high-frequency approximations and measurements.

KEY WORDS
Electromagnetic scattering, Uniform theory of diffraction, Mathieu functions

1 Introduction

The problem of the scattering by a strip was previously considered by many authors and a list of references can be found in [1]. Preliminary results for a metallic plane with a strip, or ridge, between isorefractive materials were presented in [2]. The geometry of Fig. 1 was analyzed in [3] under the assumption of plane wave incidence. In this work, the geometry of Fig. 1 is considered for a time-harmonic line source incidence, where the time-dependence factor $\exp(j\omega t)$ is omitted throughout.

2 Geometry of the problem

This is a two-dimensional problem whose cross section is shown in Fig. 1. The axis $x = 0$ is a perfect electric conductor (p.e.c.) plane and the segment OA is also a p.e.c. The points$A$ and B are the foci of an elliptic coordinate system with focal distance d. The relationship between elliptic cylinder and rectangular cartesian coordinates is $x = d/2 \cosh u \cos v$, $y = d/2 \sinh u \sin v$, $z = z$, where $0 \le u < \infty$, $0 \le v \le 2\pi$. It is also convenient to introduce the variables (ξ, η, z) defined by $\xi = \cosh u$, $\eta = \cos v$, where obviously $\xi \ge 1$, $-1 \le \eta \le 1$.

The coordinate surfaces with constant ξ are cylinders of elliptic cross-section with foci at A and B. Coordinate surfaces with constant η are hyperbolas with the same foci. When $\xi = 1$, each value of η defines a point (ξ, η) that falls on the segment of the x axis between the foci A and B. Similarly, if $\eta = 1(-1)$, each value for ξ, where $\xi > 1$, defines a point (ξ, η) on the segment of the x axis in the interval $x > d/2 (x < -d/2)$. The positive portion of the y axis corresponds to $v = \pi/2$ and the negative portion, to $v = -\pi/2$. The formulas in subsequent sections contain the dimensionless quantity $c = kd/2$. The inverse transformation from cartesian coordinates (x, y) to elliptic coordinates (ξ, η) is reported here for convenience:

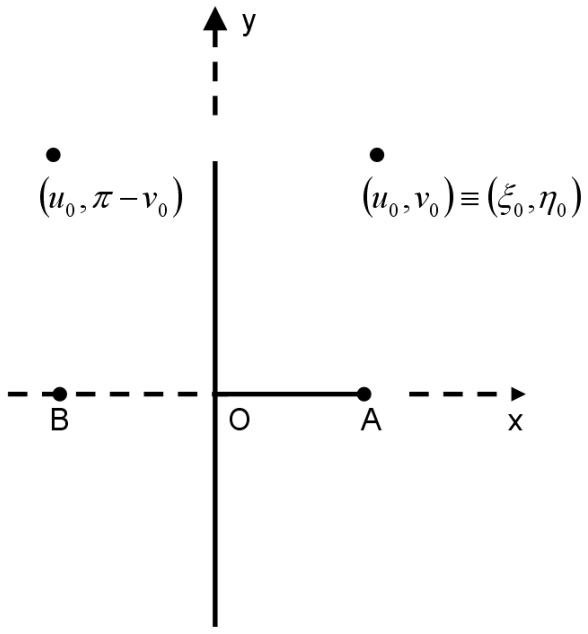

Figure 1. Geometry of the problem showing a line source at $(u_0, v_0) \equiv (\xi_0, \eta_0)$ and its image, $(u_0, \pi - v_0)$, with respect to the ground plane located at $x = 0$.

$$\xi = \sqrt{\frac{4(x^2+y^2) + d^2 + \sqrt{16(x^2+y^2)^2 + d^4 - 8d^2(x^2-y^2)}}{2d^2}} \tag{1}$$

$$\eta = \frac{2x}{d\xi}. \tag{2}$$

The notation for the Mathieu functions that are used in the following sections is taken from [4].

3 E polarization

Consider a line source parallel to the z-axis and located at the elliptic coordinates $(\xi_0, \eta_0) \equiv (u_0, v_0) \equiv (x_0, y_0)$, whose primary electric field is

$$\underline{E}^i = \hat{z} E_z^i = \hat{z} H_0^{(2)}(kR), \tag{3}$$

where k is the wavevector and

$$R = \sqrt{(x - x_0)^2 + (y - y_0)^2} \tag{4}$$

is the distance between the line source and the observation point $(x, y) \equiv (u, v) \equiv (\xi, \eta)$. The incident field may be expanded in a series of elliptic cylinder functions [1]:

$$E_z^i = H_0^{(2)}(kr) = 4 \sum_{m=0}^{\infty} \frac{1}{N_m^{(e)}} \mathrm{Re}_m^{(1)}(c, \xi_<) \mathrm{Re}_m^{(4)}(c, \xi_>) \mathrm{Se}_m(c, \eta_0) \mathrm{Se}_m(c, \eta) + \frac{1}{N_m^{(o)}} \mathrm{Ro}_m^{(1)}(c, \xi_<) \mathrm{Ro}_m^{(4)}(c, \xi_>) \mathrm{So}_m(c, \eta_0) \mathrm{So}_m(c, \eta), \tag{5}$$

where $\xi_<(\xi_>)$ means the smaller (larger) between ξ_o and ξ. Initially, one assumes that the ridge is absent so that the reflected field is given by an expression similar to (5), where the image of the source is located at $(-x_0, y_0) \equiv (u_0, \pi - v_0)$, as shown in Fig. 1. The total geometrical optics field is

$$E_z^i + E_z^r = 8 \sum_{l=0}^{\infty} \frac{\mathrm{Re}_{2l+1}^{(1)}(c, \xi_<) \mathrm{Re}_{2l+1}^{(4)}(c, \xi_>)}{N_{2l+1}^{(e)}} \mathrm{Se}_{2l+1}(c, \eta_0) \mathrm{Se}_{2l+1}(c, \eta) + \frac{\mathrm{Ro}_{2l}^{(1)}(c, \xi_<) \mathrm{Ro}_{2l}^{(4)}(c, \xi_>)}{N_{2l}^{(o)}} \mathrm{So}_{2l}(c, \eta_0) \mathrm{So}_{2l}(c, \eta). \tag{6}$$

With the ridge present, the total field is given by

$$E_z = E_z^i + E_z^r + E_z^s \tag{7}$$

where the scattered field E_z^s represents a perturbation to the geometrical optics field (6) and is written as:

$$E_z^s = 8 \sum_{l=0}^{\infty} \frac{a_{2l+1}^{(e)}}{N_{2l+1}^{(e)}} \mathrm{Re}_{2l+1}^{(4)}(c, \xi) \mathrm{Se}_{2l+1}(c, \eta_0) \mathrm{Se}_{2l+1}(c, \eta) + \frac{a_{2l}^{(o)}}{N_m^{(o)}} \mathrm{Ro}_{2l}^{(4)}(c, \xi) \mathrm{So}_{2l}(c, \eta_0) \mathrm{So}_{2l}(c, \eta) \tag{8}$$

The modal coefficients are obtained by applying the boundary conditions along the metal surfaces using the properties reported in [5], [6], which yield

$$a_{2l+1}^{(e)} = -\frac{\mathrm{Re}_{2l+1}^{(1)}(c, 1) \mathrm{Re}_{2l+1}^{(4)}(c, \xi_0)}{\mathrm{Re}_{2l+1}^{(4)}(c, 1)} \tag{9}$$

$$a_{2l}^{(o)} = 0 \tag{10}$$

4 H polarization

Consider a magnetic line source parallel to the z-axis and located at the elliptic coordinates $(\xi_0, \eta_0) \equiv (u_0, v_0) \equiv (x_0, y_0)$, whose primary magnetic field is $\underline{H}^i = \hat{z} H_z^i = \hat{z} H_0^{(2)}(kR)$.

Similar to the E-polarization case, the incident field due to the magnetic line source may be expressed as a series of Mathieu functions. When the ridge is absent, the total geometrical optics field is:

$$H_z^i + H_z^r = 8 \sum_{l=0}^{\infty} \frac{\mathrm{Re}_{2l}^{(1)}(c, \xi_<) \mathrm{Re}_{2l}^{(4)}(c, \xi_>)}{N_{2l}^{(e)}} \mathrm{Se}_{2l}(c, \eta_0) \mathrm{Se}_{2l}(c, \eta) + \frac{\mathrm{Ro}_{2l+1}^{(1)}(c, \xi_<) \mathrm{Ro}_{2l+1}^{(4)}(c, \xi_>)}{N_{2l+1}^{(o)}} \mathrm{So}_{2l+1}(c, \eta_0) \mathrm{So}_{2l+1}(c, \eta) \tag{11}$$

With the ridge present, the total field is given by

$$H_z = H_z^i + H_z^r + H_z^s \tag{12}$$

where the scattered field H_z^d represents a perturbation to the geometrical optics (11) field and is written as:

$$H_z^s = 8 \sum_{l=0}^{\infty} \frac{b_{2l}^{(e)}}{N_{2l}^{(e)}} \mathrm{Re}_{2l}^{(4)}(c, \xi) \mathrm{Se}_{2l}(c, \eta_0) \mathrm{Se}_{2l}(c, \eta) + \frac{b_{2l+1}^{(o)}}{N_{2l+1}^{(o)}} \mathrm{Ro}_{2l+1}^{(4)}(c, \xi) \mathrm{So}_{2l+1}(c, \eta_0) \mathrm{So}_{2l+1}(c, \eta) \tag{13}$$

The application of the boundary conditions leads to

$$b_{2l}^{(e)} = 0 \tag{14}$$

$$b_{2l+1}^{(o)} = -\frac{\mathrm{Ro}_{2l+1}^{(1)'}(c, 1) \mathrm{Ro}_{2l+1}^{(4)}(c, \xi_0)}{\mathrm{Ro}_{2l+1}^{(4)'}(c, 1)} \tag{15}$$

5 Comparison with high-frequency approximations

The exact total fields given by (7) and (12) for the E and H polarizations, respectively, are approximated using a high-frequency technique, the uniform theory of diffraction (UTD) [7], [8]. The high-frequency approximation is obtained by removing the metal plane $x = 0$, introducing the image OB of the segment OA and the image of the source. As a result, the contribution of the source towards the observation point will consist of two diffracted rays and, if a line of sight exists, a direct ray, as shown in Fig. 2. A similar set of rays must be considered also for the image of the source.

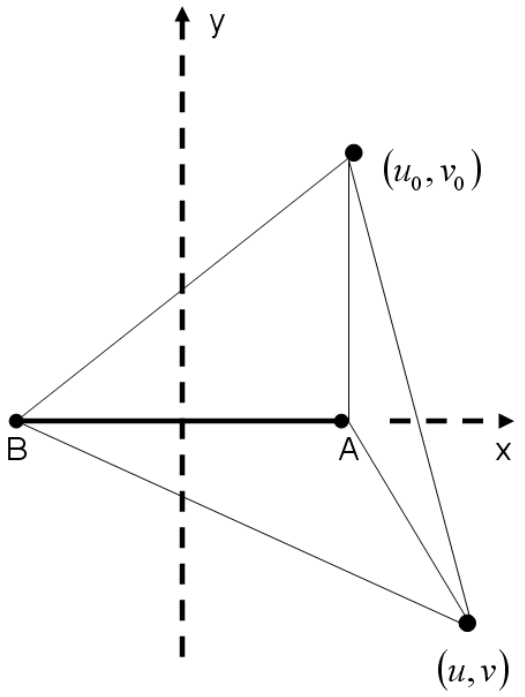

Figure 2. Geometry of the problem without the pec plane. For simplicity, this figure only shows the contribution from the original source, but another set of three ray trajectories from the image of the source needs to be accounted for to evaluate the total field at (u, v).

6 Numerical results

The numerical computations are based on some of the subroutines described in [9] and on the acceleration technique presented in [10]. Total fields are computed for three values of the parameter $c = kd/2$ that correspond to different values of the ratio d/λ. The results computed using formulas (7) and (12) are represented by a solid line, while the UTD results are represented by a dashed line. Fig. 3 shows the results for E polarization. In all three cases, the agreement between the exact theory and the high-frequency method is very good. In fact, one can hardly recognize that for each value of c two curves are actually overlapped, even though the distances among source, ridge, and observation point are only a few wavelengths. Fig. 4 shows the results for H polarization. Unlike the case of E polarization, it is possible to observe the difference between the solid and dashed line. This difference is particularly noticeable for the case $c = 1$, which correspond to a ridge that is shorter than one wavelength. When the value of c increases, the UTD approximation provides results that are closer to the exact ones.

Experiments were also conducted to compare the theoretical results given by (7) and (12) with measurements data. The antennas used in the experiments are the same

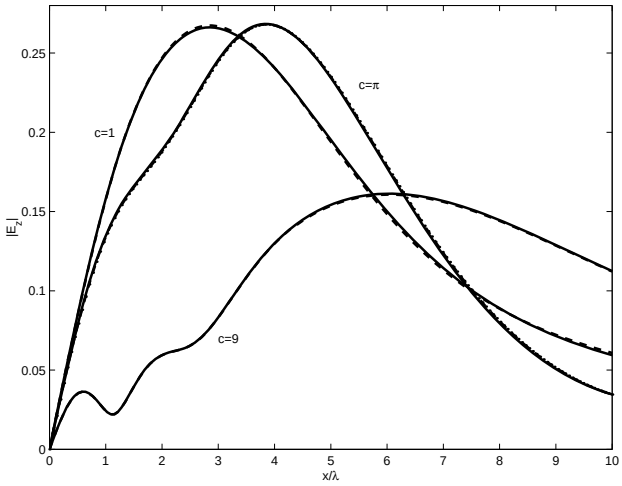

Figure 3. E polarization. Total field E_z due to a line source located at $(x_0 = \lambda/2, y_0 = 2\lambda)$ when the observation point moves along the line $(0 \leq x \leq 10\lambda, y = -3\lambda)$. The solid lines represent the exact results, while the dashed lines represent the UTD approximation.

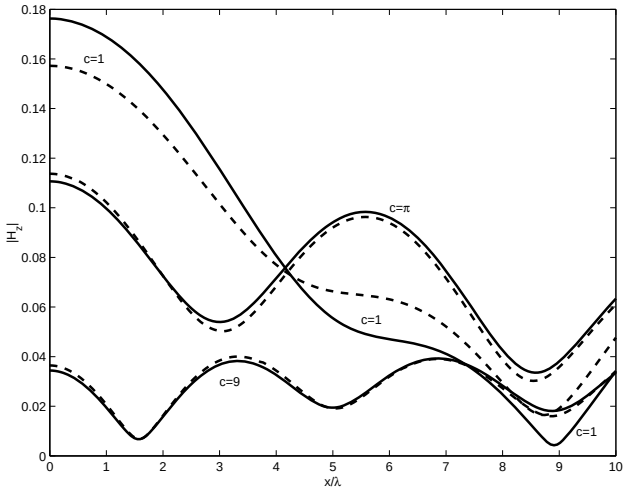

Figure 4. H polarization. Total field H_z due to a line source located at $(x_0 = \lambda/2, y_0 = 4\lambda)$ when the observation point moves along the line $(0 \leq x \leq 10\lambda, y = -10\lambda)$. The solid lines represent the exact results, while the dashed lines represent the UTD approximation.

described in [11]. Fig. 5 shows the results for the E-polarization case. One can observe a very good agreement when the distance of the observation point from the ground plane exceeds approximately 12λ. When the observation point is closer to the the ground plane the agreement is not so good and this behavior is attributed to an interaction between the antenna used in the experiment and the metallic plane. Similar conclusions may be drawn for Fig. 6.

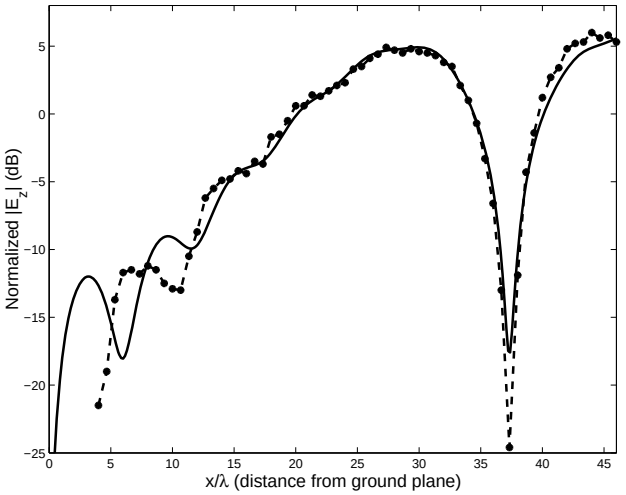

Figure 5. E polarization. Normalized value of the total field $|E_z|$ due to a line source located at $(x_0 = 6.25\lambda, y_0 = 115\lambda)$ when the observation point moves along the line $(0 \leq x \leq 46\lambda, y = -114.17\lambda)$. The solid line represents the exact results, while the dashed line represents the measurements. These results correspond to $c = 52$.

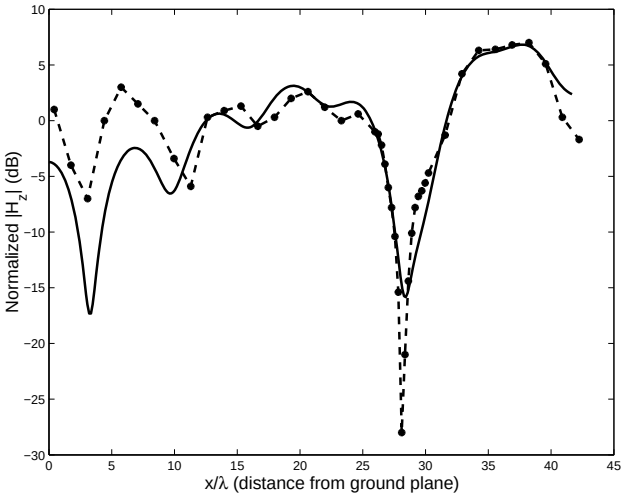

Figure 6. H polarization. Normalized value of the total field $|H_z|$ due to a line source located at $(x_0 = 6.25\lambda, y_0 = 115\lambda)$ when the observation point moves along the line $(0 \leq x \leq 42\lambda, y = -114.17\lambda)$. The solid line represents the exact results, while the dashed lines represent the measurements. These results correspond to $c = 52$.

7 Conclusions

These results are important because they present exact solutions to a new boundary value problem thus enriching the list of geometries for known canonical solutions. Additionally, the comparisons with high-frequency UTD approximations and measurements data confirm the validity of the theoretical predictions.

8 Acknowledgements

The authors are thankful to the UIC Machine shop and Prof. Constantine Megaridis for providing some instrumentation needed to take the measurements.

References

[1] J. J. Bowman, T. B. A. Senior, and P. L. E. Uslenghi, *Electromagnetic and Acoustic Scattering by Simple Shapes*, Hemisphere Publishing Corporation, New York, 1987.

[2] P.L.E. Uslenghi D. Erricolo, F. Mioc, "Exact scattering by a ridge on a metal plane with isorefractive quadrants," in *Digest of National Radio Science Meeting*, Salt Lake City, Utah, July 2000, p. 141.

[3] S. Rahman, B. Elnour, D. Erricolo, and P.L.E. Uslenghi, "Measurements and theoretical results for the scattering by a ridge on a metal plane," in *Digest of National Radio Science Meeting*, Boulder, CO, USA, Jan 2005, p. 86.

[4] J. A. Stratton, *Electromagnetic Theory*, McGraw-Hill, New York, 1941.

[5] P.L.E. Uslenghi, "Exact penetration, radiation and scattering for a slotted semielliptical channel filled with isorefractive material," *IEEE Trans. Antennas Propagat.*, vol. 52, no. 6, pp. 1473–1480, June 2004.

[6] D. Erricolo and P. L. E. Uslenghi, "Exact radiation and scattering for an elliptic metal cylinder at the interface between isorefractive half-spaces," *IEEE Trans. Antennas Propagat.*, vol. 52, no. 9, pp. 2214–2225, Sept. 2004.

[7] R. G. Kouyoumjian and P. H. Pathak, "A uniform geometrical theory of diffraction for an edge in a perfectly conducting surface," *Proc. IEEE*, vol. 62, no. 11, pp. 1448–1461, Nov 1974.

[8] C. A. Balanis, *Advanced Engineering Electromagnetics*, Wiley, New York, 1989.

[9] S. Zhang and J.-M. Jin, *Computation of Special Functions*, Wiley, New York, 1996.

[10] D. Erricolo, "Acceleration of the convergence of series containing Mathieu functions using Shanks transformation," *IEEE Antennas and Wireless Propagation Letters*, vol. 2, pp. 58–61, 2003.

[11] D. Erricolo, G. D'Elia, and P.L.E. Uslenghi, "Measurements on scaled models of urban environments and comparisons with ray-tracing propagation simulation," *IEEE Trans. Antennas Propagat.*, vol. 50, no. 5, pp. 727–735, May 2002.